

LARGER PLANET RADII INFERRED FROM STELLAR “FLICKER” BRIGHTNESS VARIATIONS OF BRIGHT PLANET HOST STARS

FABIENNE A. BASTIEN¹, KEIVAN G. STASSUN^{1,2}, JOSHUA PEPPER^{3,1}*Draft version May 6, 2014*

ABSTRACT

Most extrasolar planets have been detected by their influence on their parent star, typically either gravitationally (the Doppler method) or by the small dip in brightness as the planet blocks a portion of the star (the transit method). Therefore, the accuracy with which we know the masses and radii of extrasolar planets depends directly on how well we know those of the stars, the latter usually determined from the measured stellar surface gravity, $\log g$. Recent work has demonstrated that the short-timescale brightness variations (“flicker”) of stars can be used to measure $\log g$ to a high accuracy of ~ 0.1 – 0.2 dex (Bastien et al. 2013). Here, we use flicker measurements of 289 bright (Kepmag < 13) candidate planet-hosting stars with $T_{\text{eff}} = 4500$ – 6650 K to re-assess the stellar parameters and determine the resulting impact on derived planet properties. This re-assessment reveals that for the brightest planet-host stars, an astrophysical bias exists that contaminates the stellar sample with evolved stars: nearly 50% of the bright planet-host stars are subgiants. As a result, the stellar radii, and hence the radii of the planets orbiting these stars, are on average 20–30% larger than previous measurements had suggested.

Subject headings: Techniques: photometric — Stars: variability — Stars: planetary systems

1. INTRODUCTION

NASA’s *Kepler* Mission (Borucki et al. 2010), which monitored the brightnesses of $>150\,000$ stars, has uncovered $>3\,000$ transiting planetary candidates (Batalha et al. 2013; Burke et al. 2014). In order to measure the effective temperatures (T_{eff}) and surface gravities ($\log g$) of this large number of stars—with the core purpose of quickly identifying as many likely dwarf stars as possible and to screen out as many evolved stars as possible to achieve the primary mission goals—the mission has of necessity relied on broad-band photometry. This is the most efficient method for estimating stellar parameters, but with uncertainties in $\log g$ of 0.35–0.6 dex (Brown et al. 2011). Through community followup observations, a number of the *Kepler* targets have been observed spectroscopically, typically reducing the reported uncertainty in $\log g$ to ~ 0.1 – 0.2 dex (though with the possibility of systematic offsets up to ~ 0.4 dex; Torres et al. 2012).

Because such uncertainties in $\log g$ translate into similarly large uncertainties in the derived planet radii, many previous analyses have attempted to mitigate stellar parameter uncertainties by imposing priors based on theoretical stellar evolutionary tracks. This results in a better match of the inferred T_{eff} and $\log g$ to the theoretical main sequence, but also results in an underestimate of subgiant frequency in, e.g., the *Kepler* Input Catalog (KIC; Brown et al. 2011; Huber et al. 2014; Everett et al. 2013).

Planets orbiting bright stars are of particular interest as these offer the most opportunities for follow-

up investigation such as radial-velocity studies and in-depth spectroscopic analysis. However, magnitude-limited samples are generally not representative of the Galaxy’s underlying stellar population, one of several biases (Gaidos & Mann 2013) that affect the *Kepler* transiting planet candidates. In particular, magnitude-limited samples can be strongly biased toward stars that are intrinsically more luminous (i.e., physically larger) than the main-sequence dwarfs that comprise $\sim 85\%$ of stars in the Galaxy. Hence, it is imperative to ascertain the true $\log g$ of the stellar hosts, the bright ones especially, as accurately as possible.

Bastien et al. (2013) demonstrated that the 8-hr “flicker” (F_8) in the *Kepler* light curves can be used to measure stellar $\log g$ with an accuracy of ~ 0.1 – 0.2 dex from its correlation with granulation power (Mathur et al. 2011; Kjeldsen & Bedding 2011; Cranmer et al. 2014). Thus, $\log g$ determined from F_8 for planet-host stars can potentially significantly improve the inferred parameters of the planets. Here, we use F_8 to refine the stellar $\log g$ for the bright *Kepler* Objects of Interest (KOIs, which include both candidate and confirmed planets) with magnitudes of Kepmag < 13, and we re-examine the planet radii resulting from these revised stellar $\log g$.

2. DATA AND ANALYSIS

2.1. KOI Target Selection

We draw our bright KOI sample from the NASA Exoplanet Archive (NEA; Akeson et al. 2013) accessed on 07 Jan 2014. We restrict the sample to stars with $6650\text{ K} > T_{\text{eff}} > 4500\text{ K}$, the T_{eff} range for which F_8 is calibrated. We exclude 28 stars with overall range of photometric variability >10 ppt (parts per thousand), as phenomena in the light curves of such chromospherically active stars can boost the measured F_8 and thus result in an erroneous F_8 -based $\log g$. These excluded stars (10%

¹ Vanderbilt University, Physics & Astronomy Department, 1807 Station B, Nashville, TN 37235, USA

² Fisk University, Department of Physics, 1000 17th Ave. N, Nashville, TN 37208, USA

³ Department of Physics, Lehigh University, 16 Memorial Drive East, Bethlehem, PA, 18015

of the sample) are cooler than average for the overall sample, as expected given their large variability. Our sample after applying these cuts contains 289 stars (407 KOIs). We compare the F_8 -based $\log g$ with values from the recently published *Kepler* Stellar Properties catalog (Huber et al. 2014). Many of these values were obtained from the original KIC, whose core purpose was to ensure that as many dwarfs as possible were included among the *Kepler* targets at the risk of suffering contamination from some more evolved stars.

In Figure 1, we represent (Burger et al. 2013) these 289 planet host stars on the photometric variability evolutionary diagram introduced by Bastien et al. (2013). This diagram traces the evolution of Sun-like stars with three simple measures of their brightness variations (Basri et al. 2011): range (R_{var}), number of zero crossings (X_0), and root mean square (r.m.s.) on timescales shorter than 8 hours (8-hr “flicker” or F_8 ; see Section 2.2). Most of the KOIs orbit stars with $R_{\text{var}} < 1$ ppt, reflecting the preference for searches around magnetically quiet stars, and F_8 -based $\log g$ greater than 3.5 (indicative of dwarfs or subgiants). Some of the stars lie on the “flicker floor” and have $\log g$ as low as ~ 2.7 , making them evolved giants.

2.2. Measurement of Stellar Surface Gravity

To derive the F_8 -based $\log g$ of a star, we take all of the available PDC-MAP *Kepler* light curves and remove all known planet candidate transits using publicly available (NEA) orbital parameters. To remove remaining outlying points (flares, data artifacts, etc.), we apply a 2.5 sigma clipping to the resultant light curves. We then calculate F_8 -based $\log g$ for all light curves of the star following the methodology of Bastien et al. (2013) and take the median of the quarter-by-quarter F_8 as our robust estimate of the F_8 -based $\log g$.

In general, the quarter-to-quarter variations in the F_8 -based $\log g$ are < 0.1 dex. However, the true accuracy of the F_8 -based $\log g$ is a mild function of R_{var} (Bastien et al. 2013). Stars with $R_{\text{var}} < 1$ ppt show a constant scatter relative to the asteroseismic calibration sample of ~ 0.1 dex in $\log g$, whereas stars with $R_{\text{var}} > 1$ ppt show a slightly increased scatter of ~ 0.15 dex. Therefore, we assign an uncertainty of either 0.1 or 0.15 dex to the F_8 -based $\log g$ depending on whether the total R_{var} is less than or greater than 1 ppt.

Additionally, the asteroseismic calibration sample used in Bastien et al. (2013) only included stars brighter than $\text{Kepmag}=12$; the asteroseismic set in Huber et al. (2014) extends to $\text{Kepmag}\sim 13$ and reveals that the uncertainty in F_8 -based $\log g$ increases to ~ 0.2 dex for stars fainter than $\text{Kepmag}=12$ (Fig. 1c). We therefore increase the assigned F_8 -based $\log g$ uncertainty to 0.2 dex for $\text{Kepmag}=12$ –13. Note that the comparison to the asteroseismic sample indicates that the F_8 -based $\log g$ start to become unreliable for highly evolved giants with $\log g \lesssim 2.7$ (Bastien et al. 2013); thus in addition to restricting our analysis to the T_{eff} range of 4500–6650 K for which F_8 is calibrated, we also disregard stars with $\log g < 2.7$.

2.3. Determination of Planet Properties

To determine the planetary radius for each KOI, we begin with the NEA-reported planet-to-star radius ra-

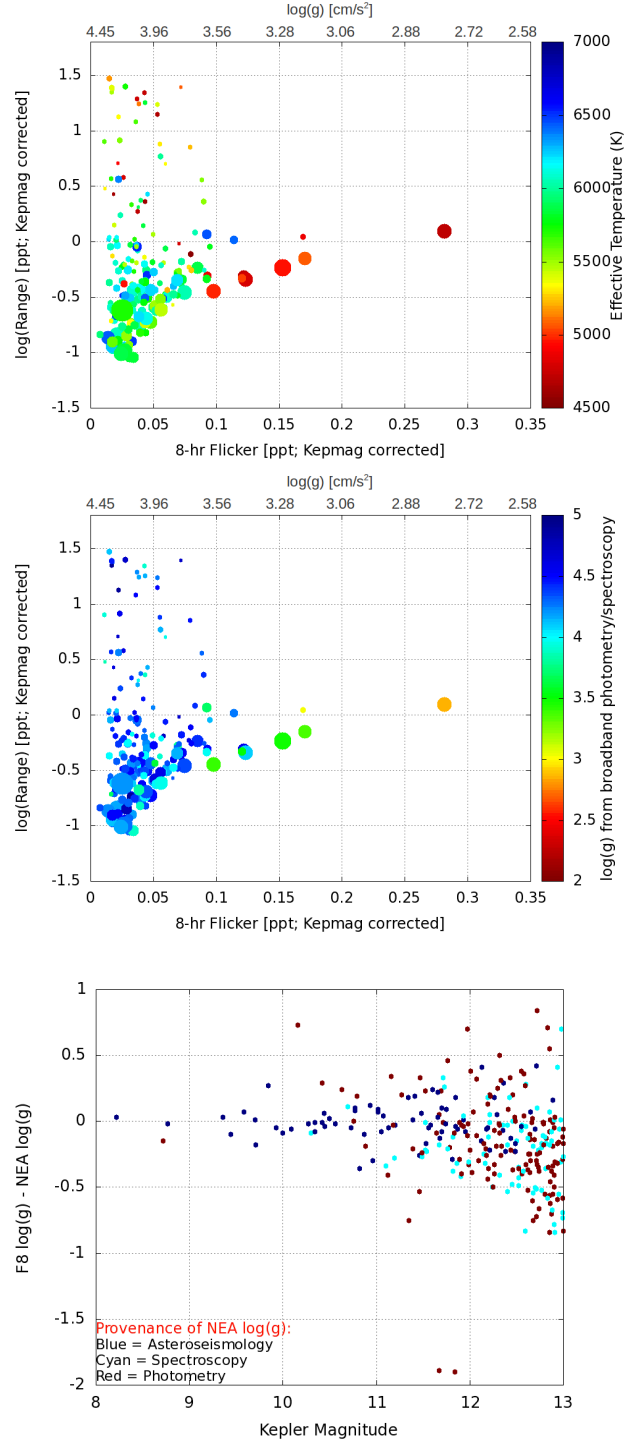


FIG. 1.— Evolutionary states ($\log g$) of KOI host stars. Top: On the abscissa is 8-h flicker (F_8) and its corresponding $\log g$ scale (Bastien et al. 2013). The amplitude of the photometric variations, R_{var} , is on the ordinate, the number of zero crossings (X_0) is represented as symbol size, and color-coded by T_{eff} (Huber et al. 2014). A large fraction of KOIs with F_8 less than 0.05 ppt (i.e., dwarfs) have $R_{\text{var}} < 1$ ppt, partially reflecting the preference for magnetically quiet stars among the KOIs. Middle: Color-coded by $\log g$ previously determined from broadband photometry/spectroscopy (NEA), the NEA $\log g$ indicate the stars are mostly dwarfs, while F_8 -based $\log g$ shows many of them are significantly more evolved. Bottom: Comparison of F_8 -based and NEA $\log g$ vs. Kepler magnitude, color-coded by method used to derive the NEA $\log g$. A color version of this figure is included in the electronic journal.

TABLE 1
STELLAR PARAMETERS FOR STUDY SAMPLE

| KIC | Kepmag | T_{eff} [K] | $\log g$ (F_8) | $\log g$ (NEA) | R_{var} [ppt] | Source ^a |
|---------|--------|-------------------------|-----------------------|-------------------|---------------------------|---------------------|
| 3109550 | 12.21 | 5449 | 4.23 | 4.03 | 4.64 | 3 |
| 3114811 | 12.81 | 6350 | 3.80 | 3.97 | 0.48 | 2 |
| 3240159 | 12.26 | 6413 | 3.95 | 4.28 | 2.40 | 3 |
| 3328080 | 12.99 | 5702 | 3.68 | 4.26 | 0.36 | 3 |
| 3425851 | 10.56 | 6343 | 4.24 | 4.26 | 0.37 | 1 |

NOTE. — A portion of the table is shown for guidance regarding content and format. The full table is available electronically.

^a Flag for source of NEA $\log g$: 1 = asteroseismic (72 stars), 2 = spectroscopic (78 stars), 3 = photometric (139 stars)

tios. For the stellar radii, we use the empirical relationship between stellar radius, T_{eff} , $\log g$, and metallicity (Torres et al. 2010), where we use NEA metallicities and T_{eff} (Huber et al. 2014) together with our newly determined F_8 -based $\log g$ values. Huber et al. (2014) used isochrone fitting to derive the NEA stellar radii from T_{eff} , metallicity, and $\log g$. Torres et al. (2010) showed that stellar masses and radii resulting from the empirical relations agree with those of model isochrones to within $\sim 5\%$. This difference in method for determining stellar radii, therefore, does not change the core results of this work.

When multiple parameter estimates are available for a given star, we favor asteroseismic parameters, followed in priority order by spectroscopy, transit analyses, and lastly broadband photometry which often includes original KIC values (note that the resulting sample contains no objects with transit-derived properties).

The result is a sample of stellar parameters that is necessarily heterogeneous but whose average accuracy in $\log g$ we expect surpasses the original KIC. We also note that the spectroscopic sample is itself heterogeneous in quality and signal-to-noise. An assessment of the individual spectra and their analysis is beyond the scope of this paper, and we consider the spectroscopic results together as an ensemble. We provide the final stellar parameters that we use, including our F_8 -based $\log g$ and the NEA parameters, in Table 1.

3. RESULTS

Comparing the $\log g$ previously estimated from broadband photometry/spectroscopy versus that newly measured via F_8 (Fig. 1c), we find the F_8 -based $\log g$ to be systematically lower (i.e., more subgiant-like), with a median difference of ~ 0.2 dex (r.m.s. of 0.3 dex for spectroscopy, 0.4 dex for photometry). In contrast, the subset of the stars with $\log g$ determined asteroseismically agrees with the F_8 -based $\log g$ to 0.02 dex in the median (r.m.s. of 0.15 dex), consistent with the expected accuracy of the F_8 -based $\log g$ (Sec. 2.2). While the scatter of 0.3–0.4 dex in the spectroscopic/photometric $\log g$ is consistent with the expected precision of photometry, it is large compared to that expected of spectroscopy. The asteroseismic and F_8 -based $\log g$ together appear to indicate a significant overestimate of the NEA $\log g$ for the bright KOI stars (the overestimate increasing to fainter magnitudes; Fig. 1c). We stress that we also find this overestimate for a number of stars whose NEA $\log g$ is

spectroscopically derived. This result has also been reported in asteroseismic studies, and may be due to biases in spectroscopic analyses that impact the $\log g$ determined for giants and subgiants (see, e.g., Huber et al. 2013, for a discussion).

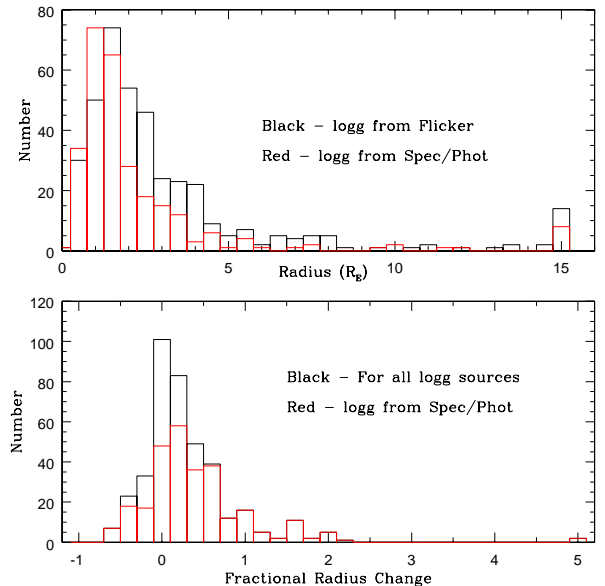


FIG. 2.— Distribution of planet candidate radii, according to $\log g$ from F_8 . Top: Distribution of planet orbital period against exoplanet radius. The arrows depict how planet radii shift when they have $\log g$ derived from F_8 (arrow head) vs. $\log g$ estimated from broad-band photometry/spectroscopy (arrow tail). Middle: The distribution of exoplanetary radii with stellar $\log g$ obtained from F_8 (black curve) and broad-band photometry/spectroscopy (red curve). Bottom: Fractional change in planet radius between F_8 -based $\log g$ and photometry/spectroscopy-based $\log g$. Using F_8 -based stellar $\log g$ results in exoplanet radii that are ~ 20 – 30% larger than suggested by broad-band photometric/spectroscopic $\log g$. A color version of this figure is included in the electronic journal.

The key effect of including F_8 -derived $\log g$ is to significantly increase the median radius of the bright KOIs (Figure 2). We find that the median KOI radius is larger by 20–30% compared to that inferred using the $\log g$ previously estimated from broadband photometry or spectroscopy, though a number of objects show a more modest or even negative change in radius (Figure 2b).

To compare our results with those expected based on the underlying stellar population, given the magnitude-limited nature of the sample, we simulated the *Kepler* field using the TRILEGAL Galactic population synthesis model (Girardi et al. 2005). We used the default TRILEGAL model parameters, for a 1 deg² line-of-sight toward the center of the *Kepler* field, and we include only simulated stars down to $\text{Kepmag} < 13$ and with $6650 \text{ K} > T_{\text{eff}} > 4500 \text{ K}$, as for the KOI sample.

Fig. 3a shows the H-R diagram of the simulated population compared with the actual KOI sample using F_8 -based (Fig. 3b) and NEA (Fig. 3c) $\log g$ values. We retain the full set of ~ 1200 stars produced by the TRILEGAL simulation to visually preserve the detail of the parameters; the actual sample with ~ 300 stars necessarily appears sparser. By construction, the simulated sample

closely traces the theoretical evolutionary tracks, with both a tight main-sequence population along the bottom and a large red giant population at upper right being most prominent, as expected for a magnitude-limited population including a mix of stellar masses and ages. For stellar masses $\gtrsim 1 M_{\odot}$, the simulated sample also includes a large population of modestly evolved subgiants with masses $\sim 1\text{--}2 M_{\odot}$, forming a thick but well defined horizontal band with $3.5 < \log g < 4.1$.

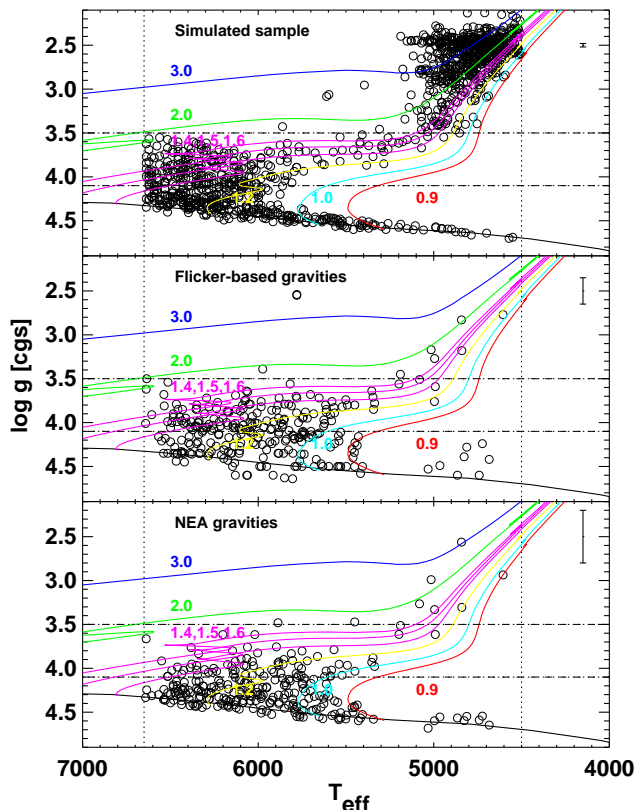


FIG. 3.— *H-R diagram of KOI host stars with $\log g$ derived from F_8 (middle) and broadband photometry/spectroscopy (bottom), and as predicted by a TRILEGAL (Girardi et al. 2005) simulation (top). Colored curves represent the theoretical evolutionary tracks (masses labeled in M_{\odot}). Vertical lines demarcate the range of T_{eff} considered in this study. The horizontal lines demarcate the range of $\log g$ for subgiants ($3.5 < \log g < 4.1$). A representative error bar on $\log g$ for each stellar sample is in the upper right of each panel. We find that the F_8 -based $\log g$ distribution more closely matches expectation than previous $\log g$ measurements, particularly in the subgiant domain, perhaps because F_8 involves no main-sequence prior on the F_8 -based $\log g$ values (see text). A color version of this figure appears in the electronic journal.*

By comparison, the observed *H-R* diagram (middle or bottom panel) lacks the highly evolved red giants ($\log g < 3$) present in the simulated sample, the result of their systematic removal by the *Kepler* mission (Batalha et al. 2010). Additionally, there is a noticeable dearth of mid-F type stars with $T_{\text{eff}} \gtrsim 6500$ K, as well as late-K type stars with $T_{\text{eff}} \lesssim 4700$ K, among the observed KOI sample, likely the result of the *Kepler* target selection process that strongly favored late-F to early-K type dwarfs for $\text{Kepmag} < 13$ (Batalha et al. 2010). For stars with $6500 \text{ K} > T_{\text{eff}} > 4700 \text{ K}$ and $\text{Kepmag} < 13$, the *Kepler* target sample should be representative of the field for all but evolved giants with $\log g < 3.5$ (Batalha et al. 2010).

More importantly, in the *H-R* diagram using $\log g$ previously estimated from broadband photometry/spectroscopy (bottom panel) the KOI sample overall follows the main sequence very closely, with few apparent subgiants with $\log g < 4.1$. With the exception of a few cool stars beginning their ascent up the red giant branch (at $T_{\text{eff}} \sim 5000$ K and $\log g \sim 3.5$), there are apparently very few of the warmer, $\sim 1\text{--}2 M_{\odot}$ subgiants with $\log g$ as low as 3.5 that are expected from the simulated sample.

In contrast, the *H-R* diagram using F_8 -based $\log g$ matches the simulated stellar population more closely. In particular, the subgiant population predicted by the simulated sample is more clearly present. Indeed, the F_8 -based $\log g$ values extend down to, but cleanly truncate at, $\log g \approx 3.5$ for $T_{\text{eff}} \gtrsim 5200$ K, just as in the simulated population. At higher $\log g$, the F_8 -based $\log g$ also trace the slope of the main sequence, with a scatter generally within $\sim 1\sigma$ of that expected for the F_8 -based $\log g$ ($0.1\text{--}0.2$ dex). Note that the F_8 -based $\log g$ are not forced to match isochrones and more generally have no priors applied to the resulting $\log g$'s.

At the same time, the F_8 -based *H-R* diagram does not perfectly match the simulated sample. For example, for stellar masses $\lesssim 1 M_{\odot}$, the F_8 -based *H-R* diagram includes a few stars that appear elevated by $1\text{--}2\sigma$ relative to the main sequence (e.g., at $T_{\text{eff}} \sim 4800$ K and $\log g \sim 4.3$). Since stars less massive than $\sim 0.9 M_{\odot}$ cannot be evolved, these stars should be firmly on the main sequence. The NEA $\log g$ values in this region of the *H-R* diagram appear better behaved, a consequence of the prior that is imposed in most photometric/spectroscopic $\log g$ analyses to force the stellar parameters to match theoretical isochrones (e.g., Huber et al. 2014). The F_8 method imposes no prior on the $\log g$ values, and so it is not surprising that for some stars the inferred $\log g$ may scatter by $1\text{--}2\sigma$ into “forbidden” regions of the *H-R* diagram. This may also be partially a result of the fact that F_8 is fundamentally calibrated to the *Kepler* asteroseismic sample and to the Sun (Bastien et al. 2013), such that F_8 -based $\log g \gtrsim 4.5$ constitute an extrapolation from that calibration. However, we also cannot rule out the possibility that the true radii of the low-mass stars are in fact larger than predicted by theoretical main-sequence models, as recent interferometric observations of low-mass planet-host stars have found the stellar radii to frequently be larger than previously thought (see von Braun et al. 2011, 2012; Boyajian et al. 2012; von Braun et al. 2014). For example, of the six stars with masses $\sim 0.8\text{--}0.9 M_{\odot}$ included in these studies, four of them (55 Cnc, 61 Vir, ρ CrB, HD 1461) are similarly elevated above the theoretically expected main sequence (von Braun et al. 2014) for reasons that are not yet clear but which may include the effects of magnetic activity (e.g., Stassun et al. 2012). In any event, for the bright KOIs considered here with very few such low-mass stars, this issue affects $1\text{--}2\%$ of the sample.

Figure 4 shows these $\log g$ comparisons directly. Here we limit the T_{eff} range to $4700\text{--}6500$ K for which the observed *Kepler* targets should be representative of the field and therefore most directly comparable to the simulated population (see above). Again, the very large population of red giants with $\log g < 3.5$ seen in the simulated sample is conspicuously missing in the actual planet

host-star sample. Thus we compare the distributions only for $\log g > 3.5$, and we normalize the histogram of the simulated sample by the number of observed stars with $\log g > 3.5$. A two-sided K-S test gives a probability of 0.01% that the NEA $\log g$ and the $\log g$ from the simulated stellar population are drawn from the same parent sample, whereas a K-S test gives a probability of 16% that the simulated and F_8 -based $\log g$ samples are drawn from the same parent sample. The F_8 -based $\log g$ show the poorest match to the simulated distribution at the highest $\log g$, corresponding to the low-mass main-sequence dwarfs that the simulation assumes to be unevolved but for which the F_8 -based $\log g$ indicate larger radii in some cases (see above). However, the F_8 -based $\log g$ are a better match overall to the simulated sample, in particular in reproducing the expected population of subgiants. Specifically, 48% of the stars have F_8 -based $\log g$ values indicative of modestly evolved subgiants ($3.5 < \log g < 4.1$), whereas previously estimated $\log g$ values had indicated that only 27% are subgiants. In comparison, 44% of the simulated sample are subgiants, in good agreement with the 48% inferred from the F_8 analysis.

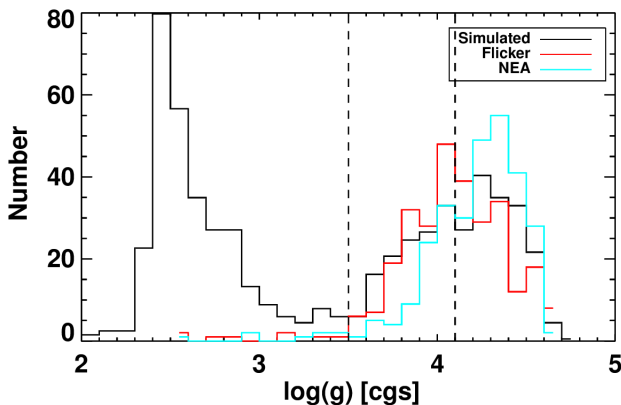


FIG. 4.— Distributions of $\log g$ for simulated (black) and KOI host stars with F_8 -based $\log g$ (red) and broadband photometry/spectroscopy-based $\log g$ (cyan). We limit the T_{eff} range here to 4700–6500 K, for which the *Kepler* targets should be representative of the field (Batalha et al. 2010). Vertical lines indicate the range of $\log g$ corresponding to subgiants. A color version of this figure appears in the electronic journal.

4. CONCLUSIONS

In this work, we used the granulation “flicker” (F_8) of bright *Kepler* planet candidate host stars to measure improved stellar $\log g$ and to thereby redetermine the planet

radii. Comparing the F_8 -based $\log g$ values with those previously published in the NEA, the latter representing a heterogeneous mix of broad-band photometric, spectroscopic, and asteroseismic methods, indicates that the stellar, and hence planetary, radii are on average 20–30% larger than suggested by the previous estimates.

The H-R diagram positions of the stars according to the F_8 -based $\log g$ in general appear better matched to the distribution from the simulated Galactic population of bright stars (Kp mag < 13) in the *Kepler* field, especially the presence of a significant population of subgiants. However, for the few very low-mass stars ($\lesssim 0.9 M_{\odot}$) in the sample, the $\log g$ values from photometry/spectroscopy appear to better match expectations as these are generally forced to match the main sequence. Whether this is a failing of the extrapolation of the F_8 - $\log g$ relation to $\log g \gtrsim 4.5$, or a manifestation of larger-than-predicted stellar radii for low-mass K and M stars as observed interferometrically (e.g., von Braun et al. 2014; Boyajian et al. 2012), remains to be determined. The performance of F_8 -based $\log g$ for very low-mass stars will be an important area for continued refinement of the F_8 technique, including its application in contexts such as astrodensity profiling (Kipping et al. 2014).

Most importantly, for a magnitude-limited sample such as that considered here, modestly evolved subgiants represent a large fraction of the population. Methods that apply a strong prior favoring main-sequence dwarf $\log g$ will systematically overestimate $\log g$ for such a sample, and in turn systematically underestimate the planet radii, particularly among the brightest stellar hosts. Our finding that broadband photometric and spectroscopic methods yield systematically larger stellar $\log g$ than asteroseismic or F_8 -based methods—especially among subgiants—is consistent with previous reports (Huber et al. 2013) but now demonstrated for a much larger sample. This bias directly impacts our understanding of the true distribution of exoplanetary radii, especially for the scientifically valuable bright systems. The results reported herein also demonstrate that one cannot ignore the magnitude-limited nature of the stellar samples when inferring their ensemble properties.

This research has made use of the NASA Exoplanet Archive, which is operated by the California Institute of Technology, under contract with the National Aeronautics and Space Administration under the Exoplanet Exploration Program. We acknowledge helpful discussions with J. Eastman. We acknowledge NSF PAARE grant AST-0849736, and NASA Harriet Jenkins and Vanderbilt Provost Graduate Fellowships.

REFERENCES

- Akeson, R. L., Chen, X., Ciardi, D. et al. 2013, *PASP*, 125, 989
- Basri, G., Walkowicz, L. M., Batalha, N. et al. 2011, *AJ*, 140, 20
- Bastien, F. A., Stassun, K. G., Basri, G., Pepper, J. 2013, *Nature*, 500, 427
- Batalha, N. M., Rowe, J. F., Bryson, S. T. et al. 2013, *ApJ*, 764, 24
- Batalha, N. M., Borucki, W. J., Koch, D. G., et al. 2010, *ApJ*, 713, L109
- Borucki, W. J., Koch, D., Basri, G. et al. 2010, *Science*, 327, 977
- Boyajian, T. S., von Braun, K., van Belle, G., et al. 2012, *ApJ*, 757, 112
- Brown, T. M., Latham, D. W., Everett, M. E., Esquerdo, G. A. 2011, *AJ*, 142, 112
- Burger, D., Stassun, K. G., Pepper, J., et al. 2013, *Astronomy and Computing*, 2, 40
- Burke, C. J., Bryson, S. T., Mullally, F. et al. 2014, *ApJS*, 210, 19
- Chaplin, W. J., Kjeldsen, H., Christensen-Dalsgaard, J. et al. 2011, *Science*, 332, 213
- Cranmer, S. R., Bastien, F. A., Stassun, K. G., Saar, S. H. 2014, *ApJ*, 781, 124
- Everett, M. E., Howell, S. B., Silva, D. R. & Szkody, P. 2013, *ApJ*, 771, 107
- Gaidos, E. & Mann, A. W. 2013, *ApJ*, 762, 41

- Girardi, L., Groenewegen, M. A. T., Hatziminaoglou, E. & da Costa, L. 2005, *A&A*, 436, 895
- Huber, D., Chaplin, W. J., Christensen-Dalsgaard, J. et al. 2013, *ApJ*, 767, 127
- Huber, D., Silva Aguirre, V., Matthews, J. M. et al. 2014, *ApJS*, 211, 2
- Kipping, D. M., Bastien, F. A., Stassun, K. G., et al. 2014, [arXiv:1403.5264](https://arxiv.org/abs/1403.5264)
- Kjeldsen, H. & Bedding, T. R. 2011, *A&A*, 529, L8
- Mann, A. W., Gaidos, E., Lépine, S. & Hilton, E. J. 2012, *ApJ*, 753, 90
- Mathur, S., Hekker, S., Trampedach, R. et al. 2011, *ApJ*, 741, 119
- Stassun, K. G., Kratter, K. M., Scholz, A., & Dupuy, T. J. 2012, *ApJ*, 756, 47
- Torres, G., Fischer, D. A., Sozzetti, A., et al. 2012, *ApJ*, 757, 161
- Torres, G., Andersen, J. & Gimnez, A. 2010, *Astron. Astrophys. Rev.*, 18, 67
- von Braun, K., Boyajian, T. S., van Belle, G. T., et al. 2014, *MNRAS*, 438, 2413
- von Braun, K., Boyajian, T. S., Kane, S. R., et al. 2012, *ApJ*, 753, 171
- von Braun, K., Boyajian, T. S., Kane, S. R., et al. 2011, *ApJ*, 729, L26